

Multiantenna GPR data acquisition design

Raul Cova, Matthew Yedlin*, David Henley, Jean-Yves Dauvignac†, Nicolas Fortino†, Kevin Hall, Christian Pichot† and Stéphane Gaffet‡

ABSTRACT

Detailed characterization of shallow sediments requires the use of very high frequency signals able to resolve fine changes in rock properties. For this reason Ground Penetrating Radar (GPR) has been chosen by the Matter-wave laser Interferometric Gravitation Antenna (MIGA) project to provide the information needed to apply near-surface corrections. Given the similitude of the physics of electromagnetic waves and seismic waves we used seismic modelling software to simulate GPR signals. The goal was to study two acquisition setups designed for the data acquisition. The original setup consisted of eight GPR transceivers, five of them spaced at 0.2m and the rest at 1m, for a maximum offset of 3.8m. This setup, despite providing a regular offset sampling was not able to provide the data needed for accurate velocity picking. For the second design the separation between the first and second group of transceivers was increased from 1m to 4m to provide a maximum offset of 6.8m. This setup provided better data for velocity picking, especially for deep events. However, under this configuration not all offsets could be sampled. The time images obtained confirm that a depth migration is needed to properly map the dip of the interfaces, especially in areas with significant lateral velocity changes. Performance of depth migration and inversion algorithms on the modelled GPR data remains to be explored.

INTRODUCTION

Ground Penetrating Radar (GPR) has been used very effectively to image the water content of the subsurface. A new opportunity for GPR has now presented itself – the use of GPR data to correct observations used in the detection of gravitational waves. This gravitational wave experiment is being built in the Vaucluse aquifer tunnels of LSBB (Low background noise inter-Disciplinary Underground Science and Technology, LSBB Underground Research Laboratory, Rustrel, France). This experiment, funded by the French research agency known as ANR, is known as MIGA -Matter-wave laser Interferometric Gravitation Antenna and is an interdisciplinary project supported by the universities of Avignon, Nice Sophia Antipolis, British Columbia (Department of Electrical and Computer Engineering) and Calgary (CREWES).

The GPR support for this project is focused on two different aspects: hardware and software. The hardware development is 90 percent complete. It includes the construction of an eight element ultra-wideband (uwb) GPR transceiver array, composed of eight tapered-slot antennas (Figure 1). These are mounted on a computer-controlled trolley. Data is collected by an 8-port vector analyzer that collects phase and amplitude frequency data for

*Department of Electrical and Computer Engineering, University of British Columbia

†Laboratoire d'Electronique, Antennes et Télécommunications (LEAT), Université Nice - Sophia Antipolis

‡Low Background Noise Inter-disciplinary Underground Science and Technology, LSBB Underground Research Laboratory



FIG. 1. Two uwb antennas. In the foreground is shown the smaller tapered slot antenna that will be used for the array trolley (Yedlin et al., 2016).

all eight GPR antennas. The acquisition system, supplied by Rohde and Schwarz, GmbH and Co KG, includes the integration of 8 high gain shielded amplifiers.

The software aspect of this project is being developed at UBC (Department of Electrical and Computer Engineering) and at the University of Calgary (CREWES). The focus is the creation of a forward modelling engine to drive the inversion of acquired data that will be used for corrections to the MIGA data. In this report we present our pilot study of generating synthetic data that conform to the surveys that will be run in the tunnels of LSBB.

NUMERICAL MODELLING

It is a formidable task to perform full synthetic data modelling for Maxwell's equations in a very large setting, with a traverse of 200m, a depth of 30m and a 0.1m shot interval comprising 64 recorded radargrams with 2000 frequency points each. The wavelength is approximately 0.33m resulting in a two-dimensional modelling panel of 600 by 90 wavelengths. If we choose a finite difference modelling tool, with 20 points per wavelength to avoid numerical dispersion, our modelling grid becomes 12000 by 1800 points – the order of 2 million grid points!

As a pilot study, we opted for a ray-tracing solution and chose the NORSAR-2D ray tracing package. Immediately the question arises regarding the mapping from electromagnetic waves to acoustic or elastic waves. We follow and augment the argument given in the paper by Laurain and Lecomte (2001). We know that in acoustic wave propagation, the acoustic impedance, Z is given as the product of density and velocity:

$$Z = \rho v. \quad (1)$$

In electromagnetic wave propagation, if we assume that we replace the density ρ by the

magnetic permeability, μ and the velocity v by $\frac{1}{\sqrt{\mu\epsilon}}$ then it is clear that, by analogy,

$$Z = \mu v = \mu \frac{1}{\sqrt{\mu\epsilon}} = \sqrt{\frac{\mu}{\epsilon}}. \quad (2)$$

The value of Z in (2) is exactly the definition of impedance in electromagnetic wave propagation and is given the symbol η .

It appears that we are now on the right track, but there is one further detail: the respective reflection coefficients in acoustic wave propagation and in electromagnetic wave propagation. To do this we need to specify the polarization of the electromagnetic wave. Following Laurain and Lecomte (2001), we note that the reflection and transmission coefficients for the TE (perpendicular to the plane of incidence polarization) correspond exactly to the acoustic case, substituting η for Z . The foregoing analysis is applied here in this pilot study to investigate the creation of a large synthetic dataset, using dynamic raytracing for simulating the data to be recorded at LSBB.

VELOCITY MODELLING

The velocity model used to compute synthetic GPR signals was based on the observations reported by Sénéchal et al. (2013). Figure 2a shows the semblance spectrum they reported and the velocity picks used to create a NMO velocity profile. These velocities were transformed to RMS velocities (Figure 2b) using the relationship $V_{NMO} = V_{RMS} / \cos(\phi)$, where ϕ is the dip angle of the interfaces. This value was set to 16° to match the apparent dip interpreted by Sénéchal et al. (2013). Finally, interval velocities were computed using Dix's equation. Figure 3 shows the structural model created by interpolating the interval velocities in Figure 2b along the structural dip. The velocity analysis on Figure 2a correspond to the lateral position $x=40\text{m}$ in the structural model.

It is important to note that the raytracing was done over a scaled version of this model. Since the desired spatial sampling was decimetric and velocities were in the order of 10cm/ns, spatial and temporal scales had to be upscaled to fit the exploration scales expected in NORSAR-2D. The scaling used was 10:1 in space dimensions, such that 10m in NORSAR-2D equals 1m on the field. The time dimension was scaled in a ratio of 1000000:1 so that 1ms in NORSAR-2D would equal 1ns on the field data. This also means that a frequency of 100Hz in the software would equal 100Mhz on the GPR data. Under this scaling a velocity of 10cm/ns on the GPR data equals 1000m/s in the software.

DATA ACQUISITION

Two data acquisition setups were considered in this study (Figure 4). The basic setup consists of a set of five finely spaced antennas, mounted on a motorized cart, while a second cart carries three more antennas with a wider spacing. The original setup (Figure 4a) provides a maximum offset of 3.8m, with antennas on the first cart spaced 0.2m and three receivers on the second cart spaced 1m. The extended setup (Figure 4b) provides a larger maximum offset by just increasing the separation between the carts from 1m to 4m, for a maximum offset of 6.8m.

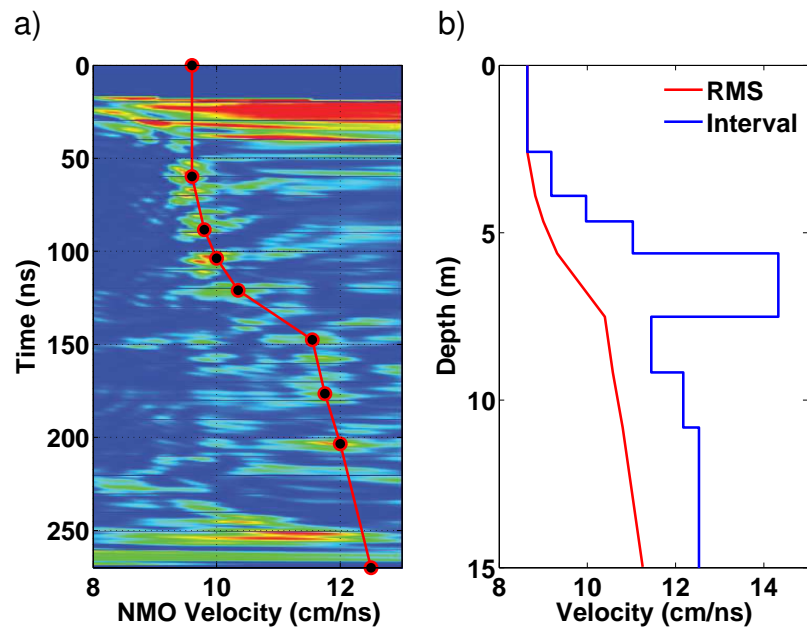


FIG. 2. a) Stacking velocities picked from Sénéchal et al. (2013) b) RMS and interval velocities computed from stacking velocities.

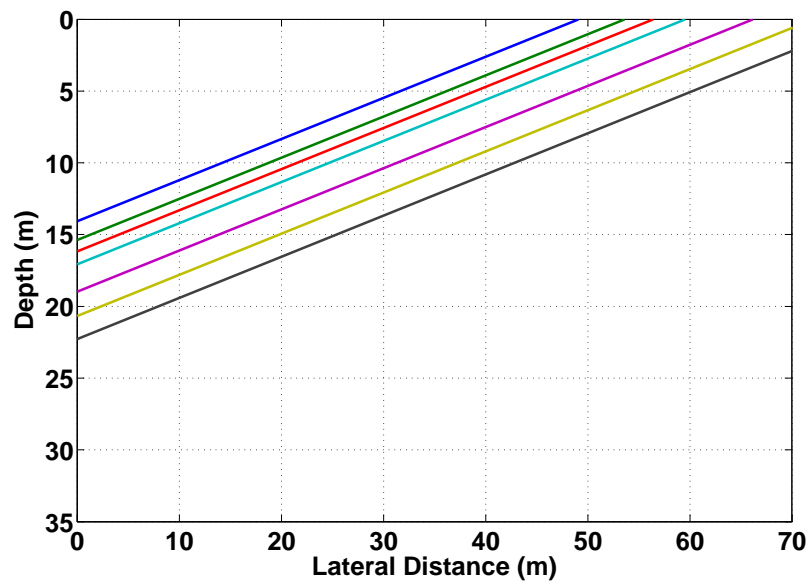


FIG. 3. Depth model used for ray tracing. Vertical exaggeration 2:1.

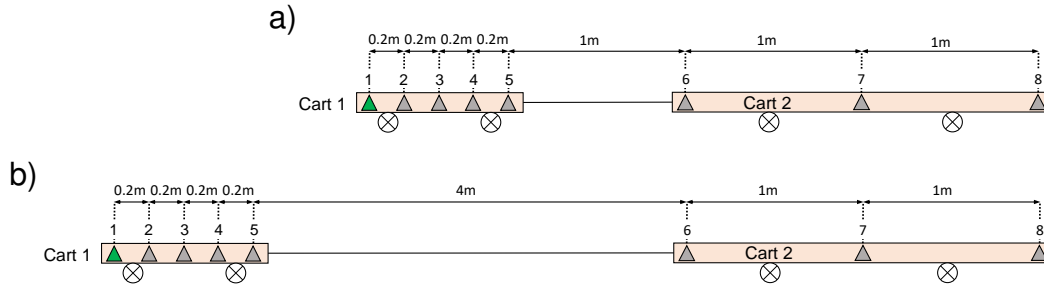


FIG. 4. Acquisition setups considered in this study. a) Original 3.8m maximum offset setup and b) extended setup with 6.8m maximum offset.

At each array location, each antenna emits a source signal that is recorded by all the antennas in the array (including the one emitting the signal). This provides a total of eight "source gathers" per array location. Then, the array is displaced 0.1m and eight more source gathers recorded.

Figure 5 displays all the offsets recorded at a fixed midpoint location after 24 displacements of the antenna array. With this setup all the offsets between 0 and 3.8m are sampled every 0.2m. This provides a total of 20 unique absolute offsets being sampled. Moreover, considering the reciprocal source-receiver pairs depicted in Figure 5 the total fold is of 39 unique signed offsets. However, due to the acquisition sequence, the same midpoint will be recorded with the same source-receiver separation but with a different source-receiver pairs, at different array locations. Figure 6 depicts how the offsets 0m, 0.2m and 0.4m get sampled several times using different source-receiver pairs. This redundancy results in a total of 64 signals being recorded with the same midpoint. Figure 7a shows the number of traces recorded at each midpoint location along the model. In Figure 7b, the offset distribution at a CMP location with full fold is displayed. Notice how the zero-offset trace is acquired eight times, i.e every time an antenna is located at that midpoint location. During the processing, traces with the same offset are usually stacked to improve S/N ratio, reducing the fold back to 39 unique signed offsets.

Figure 8 displays the fold distribution provided by the extended setup. Notice that the total fold is exactly the same as before but the fold taper segments are 3m wider (Figure 8a). Despite gaining a larger maximum offset, Figure 8b shows that there are now gaps in the offset distribution. Offsets between 1m-2m and 2m-4m are not sampled by this configuration.

DATA PROCESSING

Figure 9a displays the CMP gather recorded at $x=40\text{m}$ and its respective semblance spectrum. Notice how the areas with maximum stacking power widens at later times. This renders any velocity picking after 125ns rather inaccurate.

The CMP gather and semblance spectrum obtained with the extended setup can be seen in Figure 10. Notice that dead traces are included in the gather to represent the offset values that were not sampled. The semblance spectrum (Figure 10b) displays more focused energy at the times corresponding to each event. This provides better accuracy at the time of

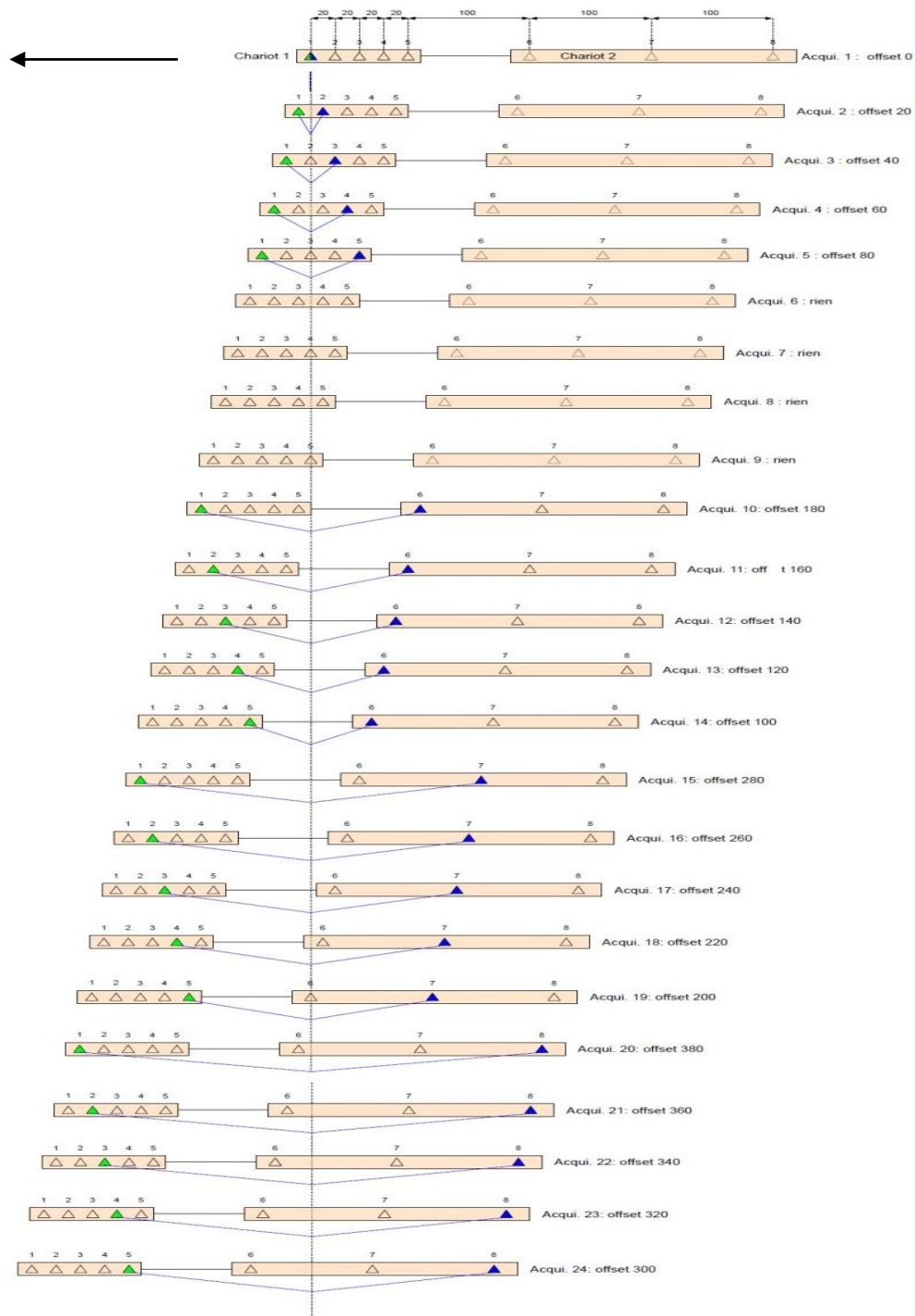


FIG. 5. Fold sketch for a fixed midpoint location considering 24 different cart positions. Only positive offsets are depicted in this figure providing a fold of 20. Including the reciprocal raypaths at each cart position the fold increases to 39. Adapted from Dauvignac (pers. comm., 2016).

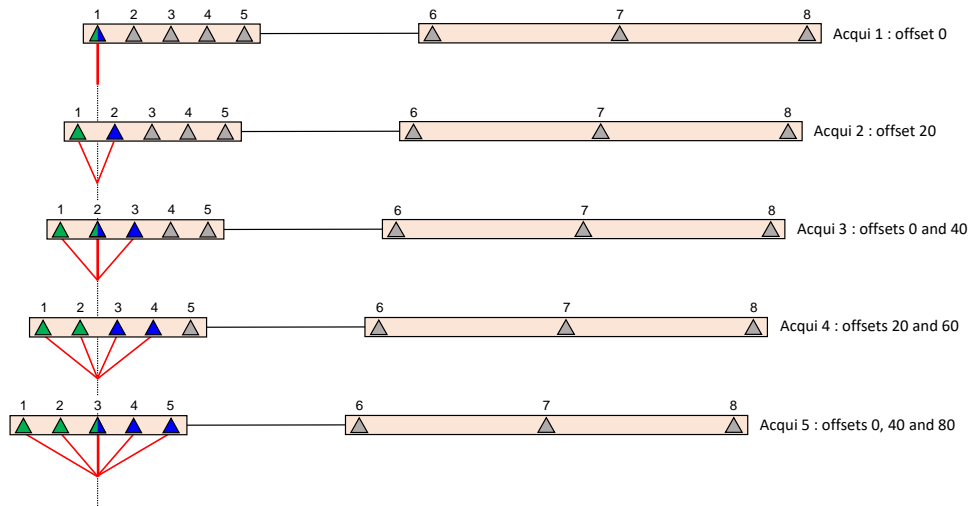


FIG. 6. Raypath for a fixed midpoint after five cart displacements. Notice that the same point gets sampled with the same offset distance but with different source-receiver pairs depending on the cart position. For example, the offset 20cm is sampled at cart position 2 using the source-receiver pair 1-2, then it gets sampled again at cart position 4 but now using the source-receiver pair 2-3.

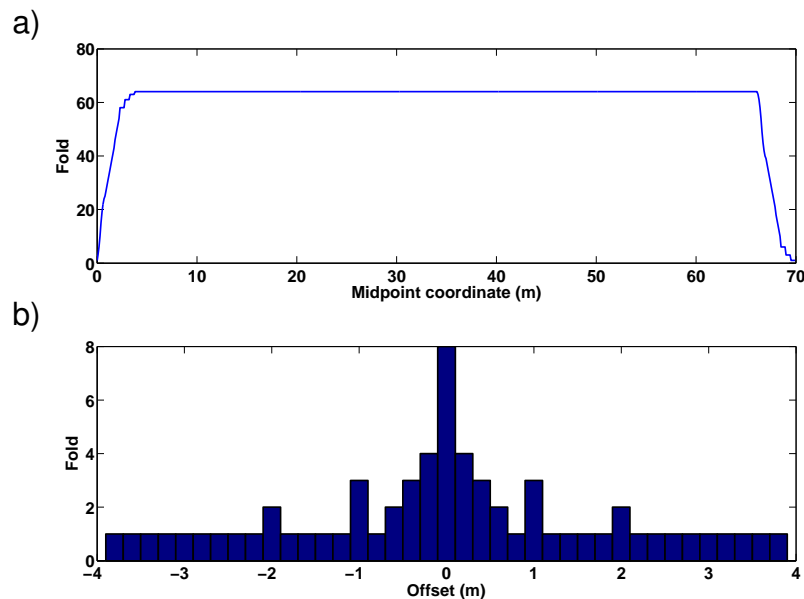


FIG. 7. a) Fold profile produced by the 3.8m array along the model. b) Offset distribution for a fixed midpoint location with full fold. Notice the redundancy in the offsets distribution specially between 0m and 1m.

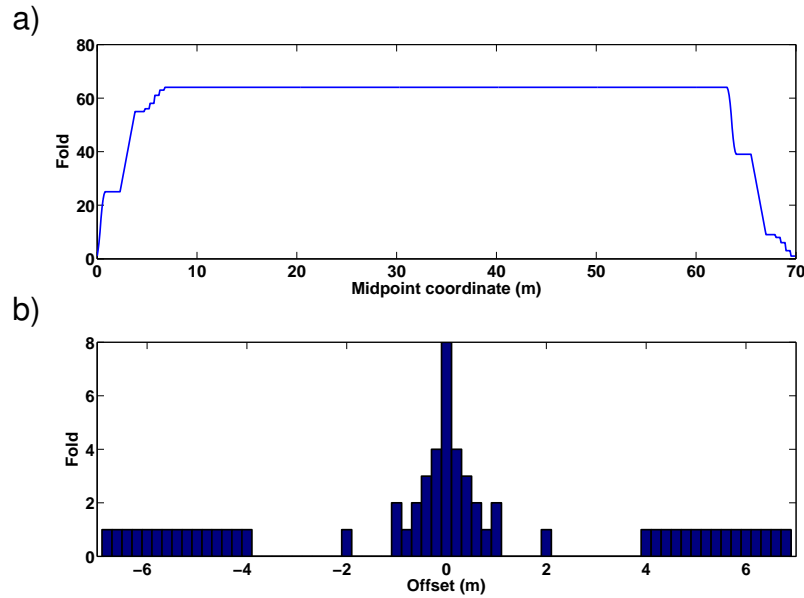


FIG. 8. a) Fold profile produced by the 6.8m array along the model. Fold taper length is now 3m wider than before. b) Offset distribution for a fixed midpoint location with full fold. The offset distribution display large gaps especially between 2m and 4m.

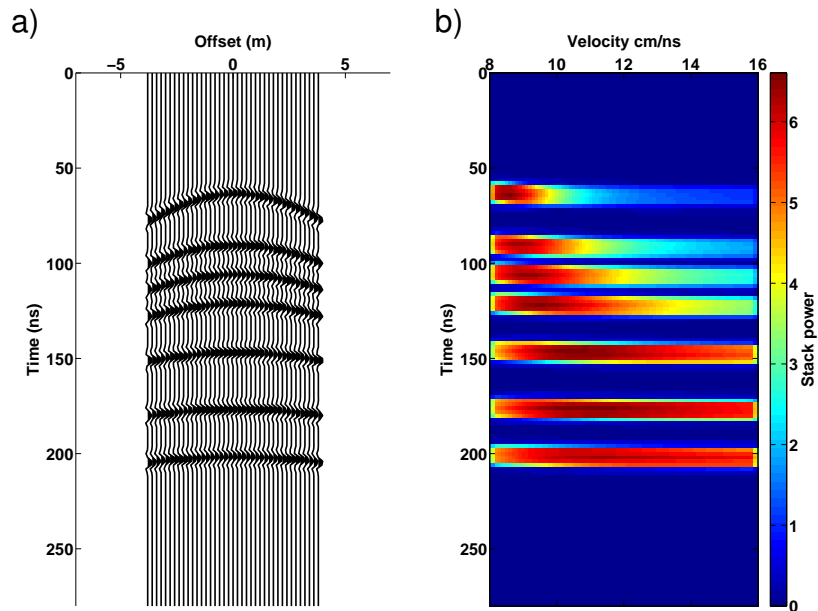


FIG. 9. a) CMP gather and b) semblance spectrum computed at the middle of the model using the 3.8m maximum offset setup. Accuracy in velocity picking deteriorates as the time of the events increase.

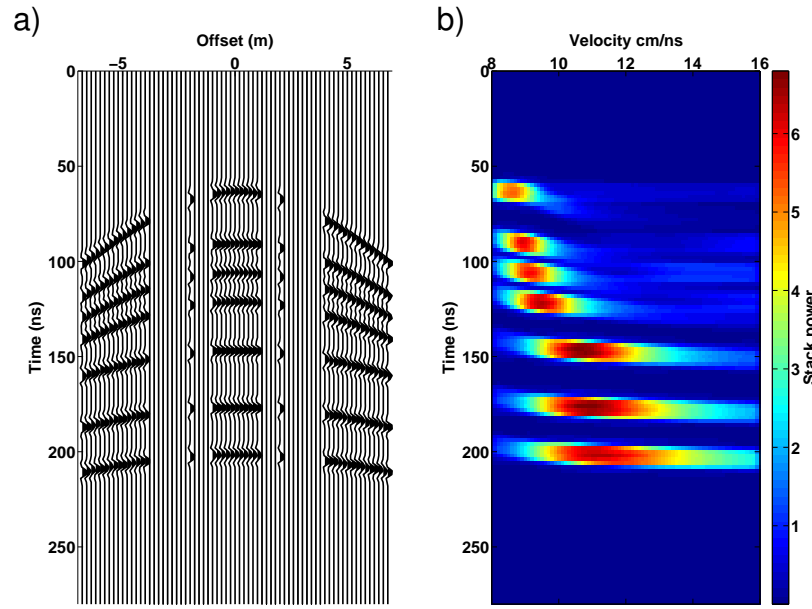


FIG. 10. a) CMP gather and b) semblance spectrum computed at the middle of the model using the 6.8m maximum offset setup. Velocity definition has improved compared to the acquisition with the 3.8m array.

picking NMO velocities. The deepest events still display wide areas of maximum stacking power, even though they are more constrained than with the original setup.

Pseudo-random noise with a S/N ratio amplitude of 1 and generated from a normal distribution with zero mean was added to each dataset. Stacked sections were computed (Figure 11) and migrated using a Kirchhoff time migration algorithm (Figure 12). As expected, the dips in the time migrated image are slightly steeper than in the stacked section. Between the x-locations 50m-70m, where the layers truncate against the surface, both time sections display deformation that are not present in the model. This is an effect of the presence of lateral changes of velocities that can not be properly accommodated by the time migration. A depth migration is needed to properly reconstruct the subsurface structure.

CONCLUSIONS

The results of this study demonstrate the viability of using a ray-tracing approach to model GPR data. Our time images are in agreement with the results reported by Sénéchal et al. (2013).

Regarding the acquisition setup, recording large offsets is key to characterize NMO velocities. The results of this study show that extending the separation between the two carts carrying the antennas provides larger offsets at the expense of an irregular offset sampling. Additional configurations could be used to gain a larger offset range keeping a regular sampling. By doubling the distance between the antennas and the cart, a maximum offset of 7.6m is possible. This configuration would provide a regular offset sampling in increments of 0.4m instead of the 0.2m given by the original design.

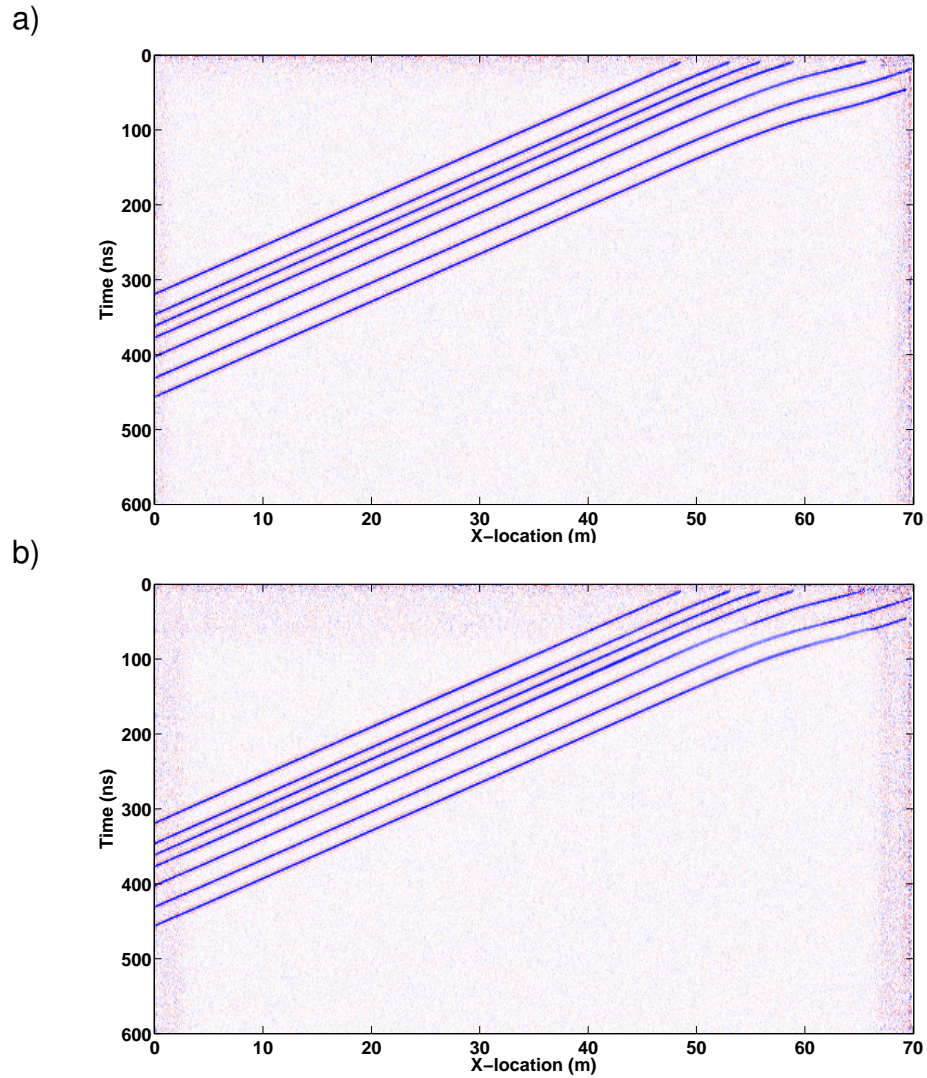


FIG. 11. Stacks obtained using the a) 3.8m and b) 6.8m maximum offset setups. No significant differences are present.

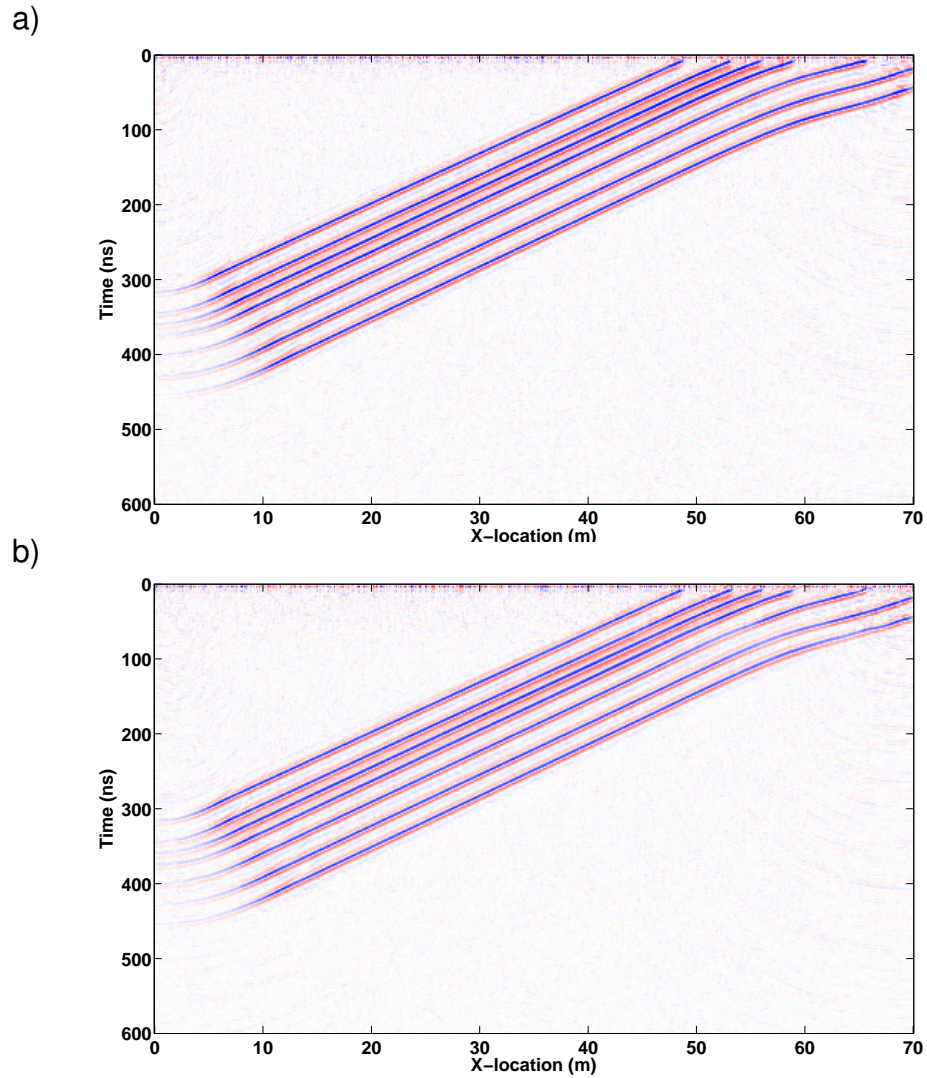


FIG. 12. Time migrated sections produced with the a) 3.8m and b) 6.8m maximum offsets. No significant differences are present.

Although the time images produced in this study did not present significant differences, the presence of lateral velocity changes, especially at the end of the line, requires a more accurate depth processing. However, to succeed in most depth migration algorithms good velocity control is needed. Data recorded at large offsets is essential for obtaining such velocities.

Furthermore, collecting data over a wide range of offsets will provide enough AVO (Amplitude Versus Offset) information to be used in future permittivity inversion algorithms. Additional data acquisition requirements for this purpose remain to be explored.

ACKNOWLEDGMENTS

The authors thank the sponsors of CREWES for continued support. This work was funded by CREWES industrial sponsors and NSERC (Natural Science and Engineering Research Council of Canada) through the grant CRDPJ 461179-13. We also acknowledge ANR (Agence Nationale de la Recherche, France) for their support and NORSAR for providing the license to use their software NORSAR-2D.

REFERENCES

- Laurain, R., and Lecomte, I., 2001, Elastic/electromagnetic wave propagation-equivalences and 2d modelling of gpr, *in* 63rd EAGE Conference & Exhibition.
- Sénéchal, G., Rousset, D., and Gaffet, S., 2013, Ground-penetrating radar investigation inside a karstified limestone reservoir: Near Surface Geophysics, **11**, No. 3, 283–291.
- Yedlin, M., Dauvignac, J.-Y., Fortino, N., Pichot, C., Cova, R., Henley, D., and Hall, K., 2016, Progress on ultra-wideband multi-antenna radar imaging for miga, *in* inter-Disciplinary Underground Science and Technology.